International Journal of Computational and Experimental Science and ENgineering (IJCESEN)

Vol. 12-No.3 (2026) pp. 167-176
http://www.ijcesen.com

ISSN: 2149-9144

Research Article

Multi-Phase Linear Induction Motor-Driven Reciprocating Pump for Advanced Photovoltaic System

Ouahid Bouakaz[1]*, Ali Bouhafs[2], Sebti Belkacem[3], Laid Khettache[4]

[1] Department of Electrical Engineering, Faculty of Applied Sciences Kasdi Merbah Ouargla University, Algeria.
* **Corresponding Author Email:** bouakaz.ouahid@univ-ouargla.dz - ORCID: 0009-0003-0576-3947

[2] Department of Electrical Engineering, Faculty of Applied Sciences Kasdi Merbah Ouargla University, Algeria.
Email: bouhafs.ali@univ-ouargla.dz- ORCID: 0000-0001-9770-1839

[3] Department of Electrical Engineering, Faculty of of Technology, University of Batna-2, Fésdis, Algeria.
Email: kbelkacem_sebti@yahoo.fr- ORCID: 0009-0009-1007-0524

[4] Department of Electrical Engineering, Faculty of Applied Sciences Kasdi Merbah Ouargla University, Algeria.
Email: khettache.laid@univ-ouargla.dz- ORCID 0000-0002-3388-3669

Article Info:

DOI: 10.22399/ijcesen.5383
Received : 10 December 2025
Revised : 25 March 2026
Accepted : 15 May 2026

Keywords

Photovoltaic
Six-Phase
Linear Induction Motor
Reciprocating Pump
Field-Oriented Control

Abstract:

This paper presents a novel design aimed at enhancing the efficiency and performance of photovoltaic (PV)-water pumping systems by integrating a reciprocating pump powered by a six-phase linear induction motor (6PLIM). The proposed motor offers greater flexibility in controlling the pump's movement, allowing for precise adjustments of flow rates and pressure levels. Furthermore, the implementation of the Perturb and Observe (P&O) Maximum Power Point Tracking (MPPT) method is necessary to maximize the output power of the PV system. The main objective of this study is to examine and evaluate the combination of the six-phase-LIM and the reciprocating pump integrated into a solar water pumping system. However, the major drawback of the linear rotor is the presence of the end-effect phenomenon, which increases the complexity of modeling and makes control difficult. To overcome this issue, a Field-Oriented Control (FOC) technique is suggested to achieve better efficiency and control flexibility of the motor. The accuracy of our proposed model is checked and validated using the Matlab/Simulink. The simulation results demonstrate that the combination of 6PLIMs with reciprocating pumps offers several advantages over traditional rotary motor-centrifugal pumps.

1. Introduction

In the agricultural irrigation field, especially in remote areas, most farmers depend on either conventional grid electricity or diesel engines to power their water-pumping systems [1-2]. However, using diesel-based systems causes noise and air pollution and relies on expensive fuel. At present, the photovoltaic water pumping system offers many advantages over traditional electric or diesel pumps, including cost-effectiveness and environmental friendliness. However, this limits their operational efficiency. Consequently, a maximum power point tracking (MPPT) technique should be implemented to maximize the power output of a solar PV system. There are different parameters and methods for MPPT discussed in literature [3]. Studies [4] have concluded that the P&O method is the most commonly used technique in practice due to its simplicity and low-cost device requirements. Furthermore, the P&O method demonstrates superior maximum power point (MPP) tracking performance compared to other techniques. The literature also addresses different types of pumps, which are typically categorized into two groups based on their operating principle: dynamic pumps and positive displacement pumps. Positive displacement pumps are utilized in applications that require a constant discharge speed, low flow rates, or high heads. Generally, these pumps are larger in size than dynamic pumps with the same capacity. As the name suggests, a reciprocating pump converts mechanical energy into pressure by using a reciprocating piston or plunger. During the suction phase, it draws water into a cylinder and during the discharge phase, it displaces the water with the force of the piston [5]. On the other hand, a six-phase induction motor consists of two sets of the stator windings placed around the stator core with a phase shift of 30 degree. This structure aims to improve performance, efficiency, and control compared to traditional three-phase motors. Besides, six-phase induction motors require a specialized power supply capable of delivering six-phase AC voltage to the stator windings. This power supply can be achieved by using multiple inverters or specialized transformers to create the required phase shift [6-7]. The rotor of a six-phase linear induction motor (6PLIM) is typically a solid conducting plate or strip that is mounted or placed close to the stator. Unlike traditional rotary motors with a rotating rotor, the rotor of a 6PLIM is usually made from materials like aluminium or copper for good electrical conductivity and mechanical strength. However, a major drawback of the linear induction motor (LIM) is the end effect phenomenon that occurs due to the motor's physical structure terminating [8]. This leads to magnetic field distortion at the ends of the motor's primary (stator). Addressing the end effect phenomenon is crucial for optimizing the performance and efficiency of linear induction motors. Various design techniques, optimization strategies, and control algorithms can be used to mitigate the effects of the end effect and enhance the overall performance of 6PLIMs in practical applications. However, controlling and operating linear induction motors pose a significant challenge with the Field-Oriented Control (FOC) technique. Theoretically, FOC aims to make the behavior of a linear induction motor similar to that of a DC motor. This can be achieved by aligning the motor flux with the d-axis (rotor flux) and adjusting the stator currents of the d- and q-axes to control the flux and force, respectively [9-12]. Furthermore, FOC typically improves efficiency, dynamic performance, and control flexibility. The main contributions of this study are as follows:

The Section II presents and describes the modeling of the PV system in detail, including the P&O-MPPT algorithm. In Section III, identifies an equivalent circuit of a 6PLIM by considering the end effect and modeling of the Field-Oriented Control (FOC) scheme. The Section IV provides a detailed mathematical formula for the single-acting reciprocating pump. The simulation results of the proposed approach are presented in Section V. Finally, Section VI concludes the paper.

1. Model Of Pv Cells and MPPT Strategy

The electrical behavior of photovoltaic (PV) cells is often described using mathematical formulas in their modeling. A widely used model is the single-diode model, which represents a PV cell using a simple equivalent circuit, as depicted in Figure.1.

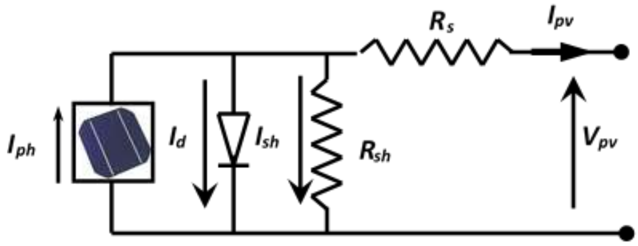

Figure 1. *Equivalent circuit of Photovoltaic cells*

The current voltage (I V) characteristics of a solar cell are described by the following's equations:

$$I_{pv} = I_{ph} - I_D - I_{SH} \quad (1)$$

$$\begin{cases} I_{pv} = I_{ph} - I_s \left[\exp(\frac{R_s.I_{pv}+V_{pv}}{V_t}) - 1\right] \\ \quad -(\frac{R_s.I_{pv}+V_{pv}}{R_{sh}}) \end{cases} \quad (2)$$

$$V_t = \frac{N_s.n.k.T}{q} \quad (3)$$

$$\begin{cases} I_D = I_s \left[\exp(\frac{R_s.I_{pv}+V_{pv}}{V_t}) - 1\right] \\ I_{SH} = (\frac{R_s.I_{pv}+V_{pv}}{R_{sh}}) \end{cases} \quad (4)$$

$$I_{ph} = N_p I_{ph-cell} \text{and} I_S = N_p I_{S-cell} \quad (5)$$

Implementing strategies for maximum power point tracking (MPPT) is crucial for enhancing the power output of a panel system. Figure.2 displays a flowchart illustrating the perturbation and observation (P&O) algorithm.

In this approach the controller adjusts the operating point by making changes to either the voltage or current of the system increasing or decreasing them accordingly. Subsequently it compares the power output post adjustment with that at the operating point. If there's an increase, in power it continues adjusting in that direction; otherwise, it changes course. This cycle repeats until reaching a predefined stopping condition [13-14].

2. Motor And Control Strategy

2.1. Model of Six-Phase LIM

In a six-phase induction motor there are usually two groups of stator windings; stator 1 and stator 2 each comprising three phases. These windings are arranged around the stator core with a 30-degree phase difference, in terms of angles. The complexity of the 6PLIM is due to the presence of six windings in the stator, which requires the park transformation into d-q synchronous form. The mutual coupling between the two sets of stator windings is neglected. Based on Duncan's approach [16], the proposed equivalent circuit model of the 6LIM, considering the phenomenon of end-effect, is illustrated in Figure.3.As depicted in Fig.3, the equivalent circuit of the 6PLIM can be divided into two parts. The first part is independent of the end-effects and represents the q-axis equivalent circuit of the induction motor. The second part is influenced by these effects and represents the d-axis, where the parameters have the end-effects,[17].

In [16], [18], Q is a significant parameter utilized to describe the end-effects phenomenon.

$$Q = \frac{D.R_r}{(L_{lr} + L_m).v} \quad (6)$$

The three-phase magnetizing inductance, which is dependent on Q, can be defined as:

$$\hat{L}_m = L_m[1 - f(Q)] \quad (7)$$

where: $f(Q) = \frac{1-e^{-Q}}{Q}$ (8)

Considering the losses caused by eddy currents, a resistance appears in the transverse branch. This resistance, denoted as $\hat{R}_r$, can be calculated as follows:

$$\hat{R}_r = R_r f(Q) \quad (9)$$

The voltage and linkage flux equations of the 6PLIM in the synchronously rotating frame for the circuits mentioned above are expressed as follows:

$$\begin{cases} V_{ds1} = R_{s1}i_{ds1} + R_r f(Q)(i_{ds1} + i_{ds2} + i_{dr}) + \frac{d\phi_{ds1}}{dt} - \omega_s \phi_{qs1} \\ V_{qs1} = R_{s1}i_{qs1} + \frac{d\phi_{qs1}}{dt} + \omega_s \phi_{ds1} \\ V_{ds2} = R_{s2}i_{ds2} + R_r f(Q)(i_{ds2} + i_{ds1} + i_{dr}) + \frac{d\phi_{ds2}}{dt} - \omega_s \phi_{qs2} \\ V_{qs2} = R_{s2}i_{qs2} + \frac{d\phi_{qs2}}{dt} + \omega_s \phi_{ds2} \\ 0 = R_r i_{dr} + R_r f(Q)(i_{dr} + i_{ds1} + i_{ds2}) + \frac{d\phi_{dr}}{dt} - \omega_{sl}\phi_{qr} \\ 0 = R_r i_{qr} + \frac{d\phi_{qr}}{dt} + \omega_{sl}\phi_{dr} \end{cases} \quad (10)$$

$$\begin{cases} \phi_{ds1} = L_{ls1}i_{ds1} + L_m\big(1 - f(Q)\big)(i_{ds1} + i_{ds2} + i_{dr}) \\ \phi_{qs1} = L_{ls1}i_{qs1} + L_m\big(i_{qs1} + i_{qs2} + i_{qr}\big) \\ \phi_{ds2} = L_{ls2}i_{ds2} + L_m\big(1 - f(Q)\big)(i_{ds2} + i_{ds1} + i_{dr}) \\ \phi_{qs2} = L_{ls2}i_{qs2} + L_m\big(i_{qs2} + i_{qs1} + i_{qr}\big) \\ \phi_{dr} = L_{lr}i_{dr} + L_m\big(1 - f(Q)\big)(i_{dr} + i_{ds1} + i_{ds2}) \\ \phi_{qr} = L_{lr}i_{qr} + L_m\big(i_{qr} + i_{qs1} + i_{qs2}\big) \end{cases} \quad (11)$$

The primary angular frequency was determined by adding the secondary angular speed to the slip frequency. This will give us:

$$\omega_s = \omega_{sl} + \omega_r \quad (12)$$

The transformation of the angular speed of the 6PLIM to a linear speed is given by

$$v = \frac{\tau_p}{\pi}\omega_r \quad (13)$$

With τ_p: is the pole pitch

In this study, the pump was directly connected to the linear motor, and the gearbox was neglected. The dynamic equation of the six-phase linear induction motor (6PLIM) is expressed as: [19]

$$M\frac{d}{dt}v + B.v = F_e - F_L \quad (14)$$

The electromagnetic force F_e applied by the motor is defined as:

$$F_e = \frac{3\pi}{2\tau_p}\frac{p}{2}\big(\phi_{dr}i_{qr} - \phi_{qr}i_{dr}\big) \quad (15)$$

and

$$F_e = \frac{3\pi}{2\tau_p}\frac{p}{2}\frac{L_m\big(1-f(Q)\big)}{L_r - L_m f(Q)}\big(\phi_{dr}i_{qs} - \phi_{qr}i_{ds}\big) = M\frac{d}{dt}v + Bv + F_L \quad (16)$$

Moreover F_L is the load force caused by the weight of the lifted water.

$$F_L = F_{pump} \quad (17)$$

2.2. Field Oriented Vector Control

The basics of Field-Oriented Control (FOC) revolve around aligning various fields, specifically the flux, which includes the stator field, rotor field, and magnetic air gap field. FOC, similar to a separately excited DC motor, aims to separate the control of torque and flux in the motor. By aligning the d-axis with the rotor flux, the control system can independently regulate the current (Iq) that generates force along the d-axis and the magnetizing current (Id) along the q-axis. Figure.4 presents the dynamic model of FOC applied to the 6PLIM, taking into account the end effect in the synchronously rotating reference frame [20]. By applying the conditions for rotor flux orientation, the rotor flux aligns with the d-axis of the d-q reference frame, and the equations for rotor flux can be expressed as follows [21]:

$$\begin{cases} \phi_{qr} = 0 \\ \phi_{dr} = \phi_r = constant \end{cases} \quad (18)$$

By substituting equation.(18) into equation.(10), the stator voltage and rotor currents are expressed as follows:

$$\begin{cases} i_{dr} = \frac{\phi_r - \hat{L}_m.i_{ds}}{L_r} \\ i_{ds} = \frac{i_{ds1} + i_{ds2}}{2} \\ i_{qr} = \frac{-L_m.i_{qs}}{L_{lr} + L_m} \\ i_{qs} = \frac{i_{qs1} + i_{qs2}}{2} \end{cases} \quad (19)$$

$$\begin{cases} V_{ds1} = \left(R_s + \hat{R}_r - \frac{\hat{R}_r.\hat{L}_m}{L_r}\right)i_{ds1} + \frac{\hat{R}_r}{L_r}\phi_r + \sigma L_s\frac{di_{ds1}}{dt} - \omega_s\sigma' i_{qs1} \\ V_{qs1} = R_s i_{qs1} + \sigma'\frac{di_{qs1}}{dt} + \omega_s\sigma L_s i_{ds1} + \omega_s\frac{\hat{L}_m}{L_r}\phi_r \\ V_{ds2} = \left(R_s + \hat{R}_r - \frac{\hat{R}_r.\hat{L}_m}{L_r}\right)i_{ds2} + \frac{\hat{R}_r}{L_r}\phi_r + \sigma L_s\frac{di_{ds2}}{dt} - \omega_s\sigma' i_{qs2} \\ V_{qs2} = R_s i_{qs2} + \sigma'\frac{di_{qs2}}{dt} + \omega_s\sigma L_s i_{ds2} + \omega_s\frac{\hat{L}_m}{L_r}\phi_r \end{cases} \quad (20)$$

With $L_r = L_{lr} + L_m[1 - f(Q)]$

The coupling voltages are defined by the back electromotive forces along the d- and q-axes in the equation provided:

$$\begin{cases} E_{d1} = -\frac{\hat{R}_r}{L_r}\phi^*{}_r + \omega_s{}^*\sigma' i_{qs1} \\ E_{q1} = -\omega^*{}_s\sigma L_s i_{ds1} - \omega^*{}_s\frac{\hat{L}_m}{L_r}\phi_r{}^* \\ E_{d2} = -\frac{\hat{R}_r}{L_r}\phi^*{}_r + \omega_s{}^*\sigma' i_{qs2} \\ E_{q2} = -\omega^*{}_s\sigma L_s i_{ds2} - \omega^*{}_s\frac{\hat{L}_m}{L_r}\phi_r{}^* \end{cases} \quad (21)$$

The equation.(22) shows that stator voltages (V_{sd1}, V_{ds2}, V_{qs1}, V_{qs2}) are directly related to stator currents

$$\begin{cases} V_{ds1}' = \left(R_s + \hat{R}_r - \frac{\hat{R}_r.\hat{L}_m}{L_r}\right) i_{ds1} + \sigma L_s\frac{di_{ds1}}{dt} \\ V_{qs1}' = R_s i_{qs1} + \sigma'\frac{di_{qs1}}{dt} \\ V_{ds2}' = \left(R_s + \hat{R}_r - \frac{\hat{R}_r.\hat{L}_m}{L_r}\right) i_{ds2} + \sigma L_s\frac{di_{ds2}}{dt} \\ V_{qs2}' = R_s i_{qs2} + \sigma'\frac{di_{qs2}}{dt} \end{cases} \quad (22)$$

$$L_s = L_{ls} + \hat{L}_m \quad (23)$$

$$\begin{cases} \sigma = 1 - \frac{\hat{L}_m^2}{L_s L_m} \\ \sigma' = (L_{ls} + L_m) - \frac{L_m^2}{(L_{lr} + L_m)} \end{cases} \quad (24)$$

In a more detailed model, the final expression of the component references of slip speed *ωsl* and the electromagnetic force can be expressed as:

$$\omega_{sl}^* = \frac{R_r.\hat{L}_m}{(L_r + L_m).\phi_r^*}\left(i_{qs1} + i_{qs2}\right) \quad (25)$$

$$\begin{cases} F_e^* = K_f . i_{qs}^* \\ K_f = \frac{3\pi}{2\tau_p}\frac{p}{2}\frac{L_m(1 - f(Q))}{L_r - L_m f(Q)}\phi_{dr}^* \\ i_{qs}^* = \frac{4\tau_p}{3\pi p}\frac{L_r - L_m f(Q)}{L_m(1 - f(Q))}\frac{F_e^*}{\phi_{dr}^*} \end{cases} \quad (26)$$

3. Single Acting Reciprocating Pump

Among the types of pumps available, positive displacement piston pumps, also known as plunger pumps, were chosen for their excellent performance in applications that need high pressure and low flow rates. These pumps consist of a cylinder housing a reciprocating plunger. During operation, water enters the pump chamber through a valve (S1) and is discharged through an outlet valve (D1) due to the movement of the piston, as shown in Figure.5 [22]. When connecting the motor to the pump, the actuator's movement corresponds to the up and down strokes of the piston. A power converter must activate the motor's phase windings in sequence, reversing this sequence each time the actuator reaches its end positions [23].

The power requirement for an acting reciprocating pump can be estimated using formulas:

$$P_p = \frac{Q_p.H.\rho.g}{\eta} \quad (27)$$

$$H = H_s + H_d \quad (28)$$

Where Pp is the power required by the pump (W), H is the total head (m), ρ is the density of the pumped liquid (kg/m3), g is the acceleration due to gravity (approximately 9.81 m/s), and η is the overall efficiency of the pump-motor system (specified in decimal degrees). These formulas provide an estimate of the power required by the pump under steady-state conditions, assuming ideal behavior. The capacity or flow rate (Qp) of a single-acting reciprocating pump can be calculated using the following formula [24]:

$$Q_p = \frac{A.L.N}{60} \quad (29)$$

where Qp is the capacity or flow rate (m3/s), A is the piston area (m2), L is the stroke length (m), and N is the pump speed (rpm).

4. Simulation Results

In order to verify and validate the proposed approach, this section carries out a simulation using MATLAB/Simulink to demonstrate the performance of the proposed design system. For this simulation, we utilized the Mega solar USA Powertec Plus 235-6PH-US with 8 series modules, 1 parallel string, and the P&O MPPT algorithm. You can find the details in Table.

Table 1. *Manufacturer Specifications For A Pv Module (Megasolar Usa Powertec Plus 235-6ph-Us).*

Pv Parameters	Value
Maximum Power	235.41 (W)
Cells per module (Ncell)	60
Open circuit voltage **Voc**	36.45 (V)
Short-circuit current **Isc**	8.37 (A)
Voltage at maximum power point	29.5 (V)
Current at maximum power point	7.98 (A)
Shunt resistance **Rsh**	1259.8 (Ω)
Series resistance **Rs**	0.2852(Ω)

Figures 6(a) and 6(b) illustrate the photovoltaic (PV) output voltage and current, respectively, under different levels of solar irradiance ranging from 700 W/m² to 1000 W/m². As observed, the output voltage of the PV array remains nearly constant at approximately 250 V, whereas the output current exhibits a significant variation. Specifically, the current increases from 5.024 A at 700 W/m² to 7.23 A at 1000 W/m². This behavior confirms the PV module's expected response to changing irradiance levels. Figure 6(c) presents the irradiance profile used in the simulation, with a constant ambient temperature of 25 °C maintained throughout the test.To demonstrate the effectiveness of the proposed FOC control method, the parameters of the

6PLIM used in this study are summarized in Table.2.

Table 2. *Six-Phase Linear Induction Motor Parameters*

Parameters	Values
Rs	1.2 Ω
Rr	2.4 Ω
Lls	0.0174 H
Llr	0.0043 H
Lm	0.0513 H
τ_p	0.15 m
D	1.31 m
p	6

Additionally, the motor was run with a reference speed (red line) in a periodic square waveform alternating between approximately 0 and 2.1 rad/s and a reference flux of 0.8 Wb. An external load force was applied, indicating that the motor is coupled to the pump (load pump) (see Fig.7(a and b)). The tracking performance of the FOC scheme is evaluated by comparing the actual motor speed (blue line) with the reference trajectory. The Figure.7. (a) indicate that the controller achieves accurate and rapid tracking. At each transition in the reference signal, the motor speed follows with steady-state error remains negligible typically within ±0.01–0.02 rad/s and minor overshoot typically less than 5%.The rotor flux responses, depicted in Figure. 8, indicate successful decoupling between the direct and quadrature components. The direct rotor flux (ϕdr) remains unaffected and is maintained constant at the reference value of ϕdr = 0.8 Wb, while the quadrature rotor flux (ϕqr) is kept at zero (ϕqr = 0 Wb). It is worth mentioning that there are significant peaks observed when the speed reference changes.

Figure.9 (a and b) presents the response of the components of the stator current, id and iq. These values are obtained by minimizing the error between the actual and reference values of force and flux. As shown, the d-axis current (ids1 and ids2) changes from (16.6 A to 12.37 A) due to a speed reference change, the q-axis current (iqs1 and iqs2) is only slightly affected and quickly recovers to its commanded value of (0.04 A). So, the decoupling between the direct and quadrature stator current was successfully achieved.

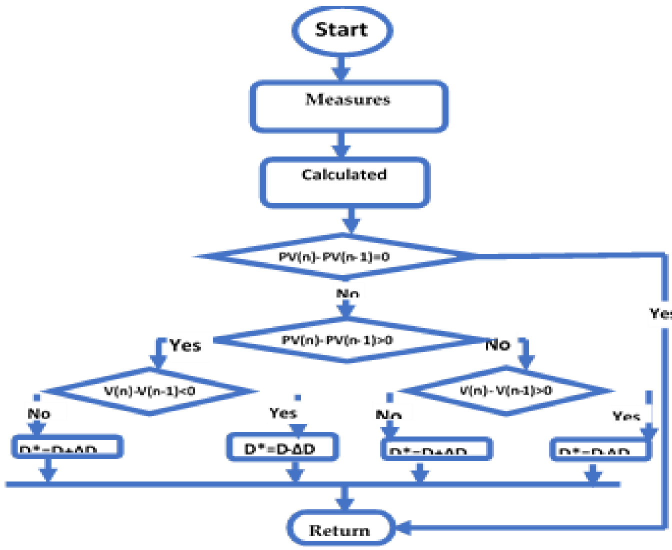

Figure 2. *Flowchart of P&O MPPT algorithm [15]*

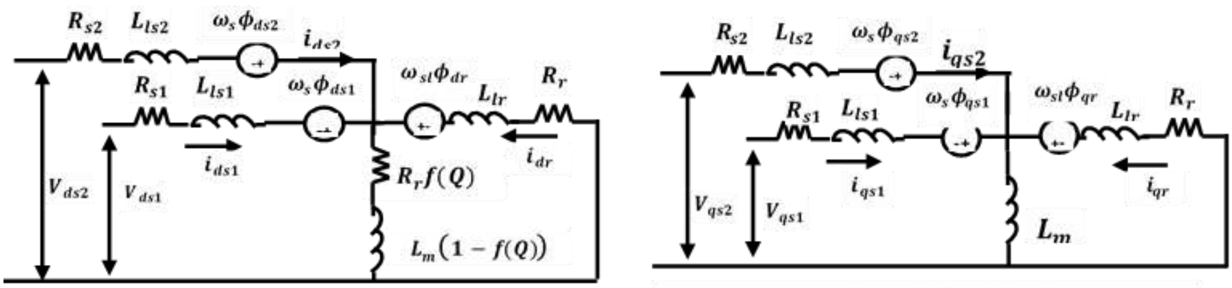

d- axis equivalent circuit *q- axis equivalent circuit*

Figure 3. *Six-phase LIM equivalent electrical circuit taking into account end-effect.*

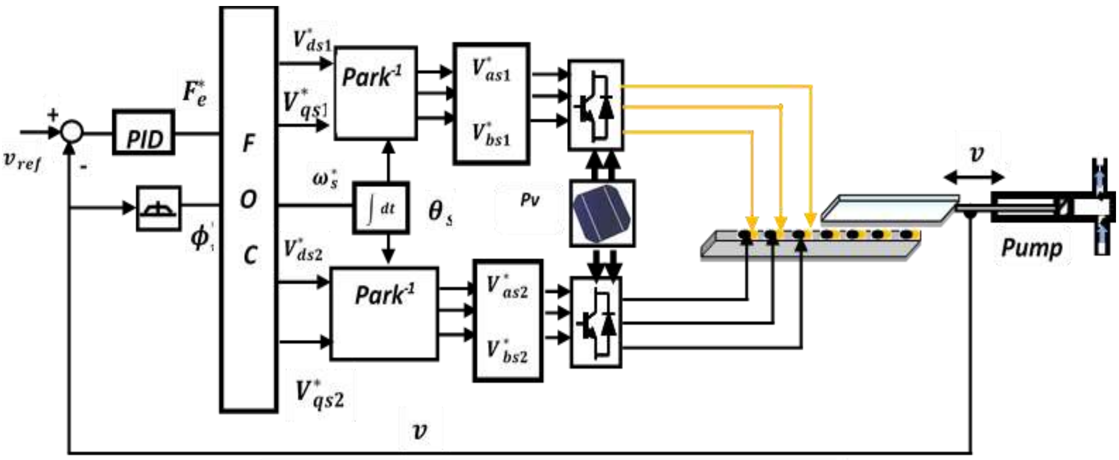

Figure 4. MATLAB/Simulink model of Solar water pump

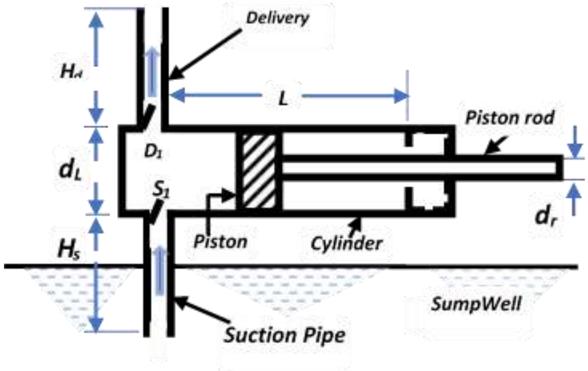

Figure 5. Main Parts of Reciprocating Pump

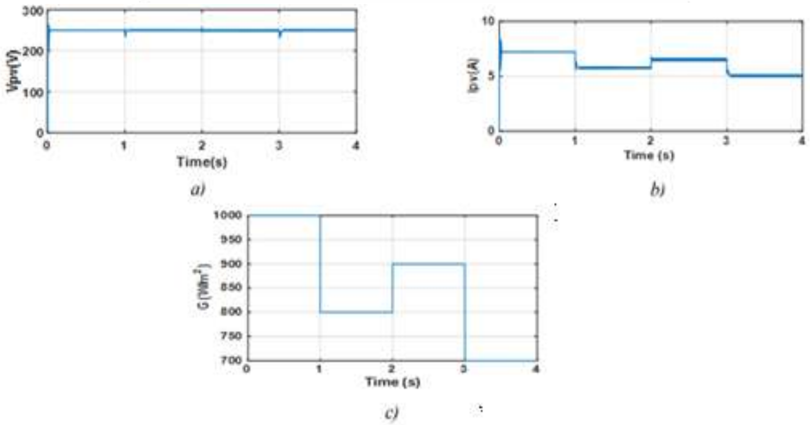

Figure 6. PV output voltage and current under varying solar irradiance

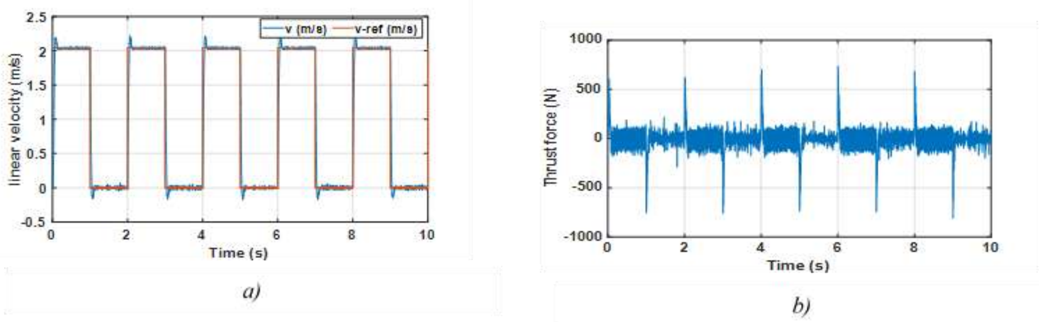

Figure 7. Speed and thrust force responses under reference speed variation

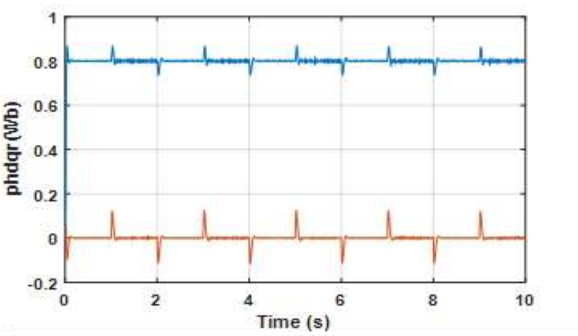

Figure 8. *Direct and Quadrature rotor flux*

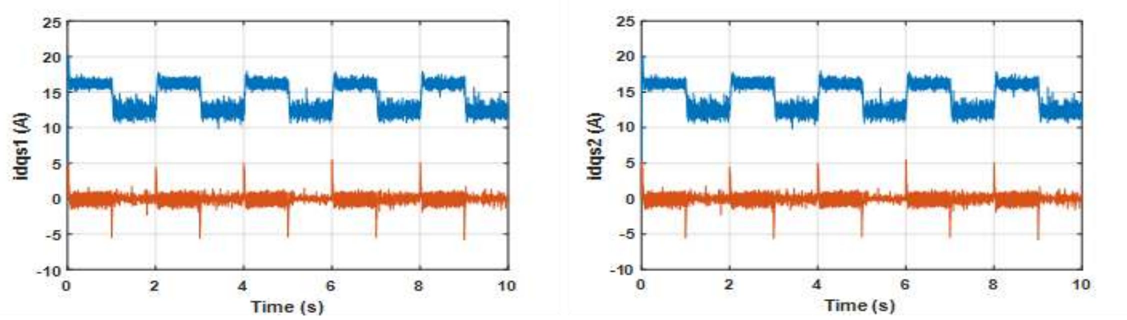

a) *b)*

Figure 9. *Direct and Quadrature components of both stator current responses.*

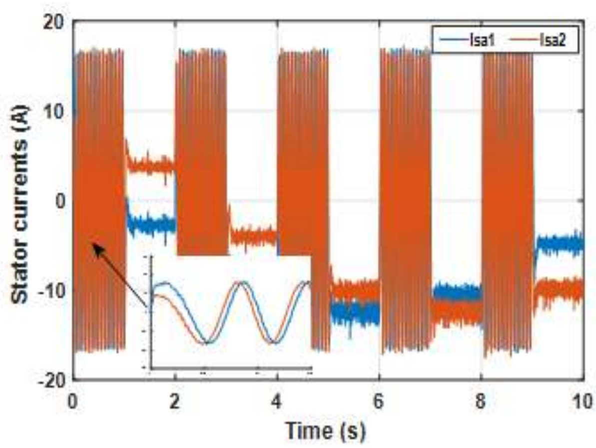

Figure 10. *Stator phase currents isa1 and isa2 with an angle α set to 30°.*

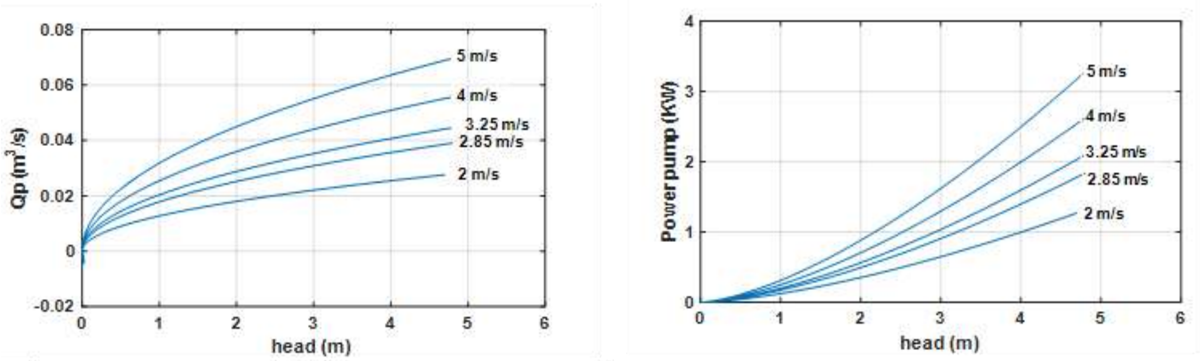

a) *b)*

Figure 11. *Pump performance curves: (a). Flow vs Head, (b) power vs Head.*

Figure.11. (a and b) demonstrate the increases in flow rate (Qp) and power of the pump for different values of Head (H) and speed. It is evident that the pump exhibits clear dependence on LIM speed, with both power and flow rate rising consistently across the head range as speed increases. The observed trends validate the coupling of LIM dynamics with pump performance, highlighting the feasibility of precise flow and power control via speed regulation. These results are particularly relevant in variable-load applications, such as water distribution, where energy-efficient control is essential. Figure.10 shows the phase currents (isa1 and isa2) in the stator windings of the six-phase linear induction motor (6PLIM) with an angle α set to 30°. The waveform symmetry and continuity demonstrate proper functioning of the six-phase inverter and stator windings under transient conditions.

6. Conclusions

This paper demonstrates the benefits of using a linear induction motor in conjunction with a reciprocating pump (SAR) to improve photovoltaic (PV)-water pumping systems. The innovative system includes a PV array, a boost converter controlled by an MPPT algorithm (Perturb & Observe), and the application of field-oriented control to a six-phase linear induction motor (6PLIM) coupled with a single-acting reciprocating pump. Based on our simulation results, the following conclusions can be drawn:

- Among the investigated PV pumping technologies, the configuration that utilizes a water hydraulic single-action reciprocating pump driven by a linear induction motor is the most cost-effective solution.

-The FOC technique proposed in this paper effectively tracks reference speed with a short response time and minimal error, even in the presence of the end-effect phenomenon. This improves the decoupling between force and flux.

-Our proposed model, compared to traditional centrifugal pumps and diesel water pumping systems, is more competitive under different conditions, such as variations in solar irradiance and head.

Therefore, successful implementation of our approach will not only provide farmers with a sustainable and cost-effective solution but also contribute to the reduction of noise, air pollution, and fuel consumption.

NOMENCLATURE

V_{ds1}, V_{qs1}:Primary voltages in the d-q axes stator1
V_{ds2}, V_{qs2}:Primary voltages in the d-q axes stator2
$i_{ds1}, i_{qs1,}2, i_{qs2,}$:d-q axes primary currents (A)
i_{dr}, i_{qr}:d-q axes Linor currents (A)
$\phi_{ds1}, \phi_{qs1}, \phi_{ds2}, \phi_{qs2}$:d-q axes Primary flux linkages (Wb)
ϕ_{dr}, ϕ_{qr}:d-q axes Linor flux linkages (Wb)
L_s, L_r:Primary and linor self-inductances (H)
R_s, R_r:Primary and linorresistances (Ω)
Q :Factor associated with the length of linor
F_e : Electromagnetic force (thrust force)
τ_p :Pole pitch (m)
D:Length of the linor (m)
p :No of poles
v:Velocity (m/s)
ω_s:Primary angular velocity (rad/sec)
ω_r:Linor angular velocity (rad/sec)
ω_{sl}:Slip frequency (rad/sec)
Qp :Flow rate (m3/s)
σ, σ' : Leakage coefficients associated to cases with and without end-effect
Ipv : Output current of the solar cell.
Iph : Photocurrent proportional to isolation.
q : Electron charge (approximately 1.602×10−19 °C).
k: Boltzmann constant (approximately 1.381×10−23 J/K).

Author Statements:

- **Ethical approval:** The conducted research is not related to either human or animal use.
- **Conflict of interest:** The authors declare that they have no known competing financial interests or personal relationships that could have appeared to influence the work reported in this paper

- **Acknowledgement:** The authors declare that they have nobody or no-company to acknowledge.

- **Author contributions:** The authors declare that they have equal right on this paper.

- **Funding information:** The authors declare that there is no funding to be acknowledged.

- **Data availability statement:** The data that support the findings of this study are available on request from the corresponding author. The data are not publicly available due to privacy or ethical restrictions.
- **Use of AI Tools:** The author(s) declare that no generative AI or AI-assisted technologies were used in the writing process of this manuscript.

References

[1] Gadiraju, H. K. V., Barry, V. R., & Jain, R. K. (2022). Improved performance of PV water pumping system using dynamic reconfiguration algorithm under partial shading conditions. *CPSS Transactions on Power Electronics and*

Applications, *7*(2), 206–215. https://doi.org/10.24295/CPSSTPEA.2022.00019

[2] Makhlouf, M., Messai, F., & Benalla, H. (2011). Vectorial command of induction motor pumping system supplied by a photovoltaic generator. *Journal of Electrical Engineering*, *62*(1), 3–10. https://doi.org/10.2478/v10187-011-0001-7

[3] Bollipo, R. B., Mikkili, S., & Bonthagorla, P. K. (2020). Critical review on PV MPPT techniques: Classical, intelligent and optimization. *IET Renewable Power Generation*, *14*(9), 1433–1452. https://doi.org/10.1049/iet-rpg.2019.1163

[4] Mao, M., Cui, L., Zhang, Q., Guo, K., Zhou, L., & Huang, H. (2020). Classification and summarization of solar photovoltaic MPPT techniques: A review based on traditional and intelligent control strategies. *Energy Reports*, *6*, 1312–1327. https://doi.org/10.1016/j.egyr.2020.05.013

[5] Zhou, Y., Zhao, J., & Liu, X. (2021). Loss minimization control of dual three-phase linear induction motor with system-level loss model. *IEEJ Transactions on Electrical and Electronic Engineering*, *16*, 324–331. https://doi.org/10.1002/tee.23300

[6] Badreddine, L., Fouad, B., & Samir, Z. (2022). Modelling and control of double star induction machine using active fault tolerant control based on backstepping controller and nonlinear adaptive observer. In *International Conference of Advanced Technology in Electronic and Electrical Engineering (ICATEEE)* (pp. 1–6). https://doi.org/10.1109/ICATEEE57445.2022.10093727

[7] Lazreg, M. H., & Bentaallah, A. (2018). Sensorless fuzzy sliding-mode control of the double-star induction motor using a sliding-mode observer. *Elektrotehniski Vestnik*, *85*(4), 169–176.

[8] Yeqing, H., Songlin, N., Kai, M., Fan, L., & Lei, L. (2015). Static stress and modal analysis of water hydraulic reciprocating piston pump driven by the linear motor. In *International Conference on Fluid Power and Mechatronics (FPM)* (pp. 914–917). https://doi.org/10.1109/FPM.2015.7337245

[9] Loukianov, A., Rivera, J., Alanis, A. Y., & Raygoza, J. J. (2012). Super-twisting sensorless control of linear induction motors. In *9th International Conference on Electrical Engineering, Computing Science and Automatic Control (CCE)* (pp. 1–5). https://doi.org/10.1109/ICEEE.2012.6421172

[10] Kang, G., & Nam, K. (2005). Field-oriented control scheme for linear induction motor with the end effect. *IEE Proceedings - Electric Power Applications*, *152*(6), 1565–1572. https://doi.org/10.1049/ip-epa:20045185

[11] Han, Y., Nie, Z., Xu, J., et al. (2020). Mathematical model and vector control of a six-phase linear induction motor with the dynamic end effect. *Journal of Power Electronics*, *20*, 698–709. https://doi.org/10.1007/s43236-020-00059-x

[12] Xingfa, S., et al. (2018). A speed sensorless control strategy for a dual three-phase linear induction motor based on SMFEKF. In *CSAA/IET International Conference on Aircraft Utility Systems* (pp. 769–775). https://doi.org/10.1049/cp.2018.0136

[13] Femia, N., Petrone, G., Spagnuolo, G., & Vitelli, M. (2005). Optimization of perturb and observe maximum power point tracking method. *IEEE Transactions on Power Electronics*, *20*(4), 963–973. https://doi.org/10.1109/TPEL.2005.850975

[14] Kumar, M., Bharti, R., & Rao, D. V. S. K. K. (2019). Conventional and hybrid perturb & observe based maximum power point tracking for solar system. In *International Conference on Visualisation Towards Emerging Trends in Communications Networks (ViTECoN)* (pp. 1–5). https://doi.org/10.1109/ViTECoN.2019.8899412

[15] Sera, D., Mathe, L., Kerekes, T., Spataru, S. V., & Teodorescu, R. (2013). On the perturb-and-observe and incremental conductance MPPT methods for PV systems. *IEEE Journal of Photovoltaics*, *3*(3), 1070–1078. https://doi.org/10.1109/JPHOTOV.2013.2261118

[16] Duncan, J. (1983). Linear induction motor equivalent circuit model. *IEE Proceedings B - Electric Power Applications*, *130*(1), 51–57. https://doi.org/10.1049/ip-b.1983.0008

[17] Khettache, L., & Abdessemed, R. (2023). A new speed control approach of linear induction motor based on robust RST controller and MRAS estimator. *International Journal of Engineering*, *36*(4), 630–639. https://doi.org/10.5829/ije.2023.36.04a.03

[18] Zhang, L., Obeid, H., Laghrouche, S., & Cirrincione, M. (2019). Second order sliding mode observer of linear induction motor. *IET Electric Power Applications*, *13*(1), 38–47. https://doi.org/10.1049/iet-epa.2018.5232

[19] Han, Y., Nie, Z., Xu, J., Zhu, J., & Sun, J. (2020). Control strategy for optimizing the thrust of a high-speed six-phase linear induction motor. *IET Power Electronics*, *13*(11), 2260–2268. https://doi.org/10.1049/iet-pel.2019.1334

[20] Gonzalez, O., Ayala, M., Rodas, J., Gregor, R., Rivas, G., & Doval-Gandoy, J. (2018). Variable-speed control of a six-phase induction machine using predictive fixed switching frequency current control techniques. In *IEEE PEDG* (pp. 1–6). https://doi.org/10.1109/PEDG.2018.8447837

[21] Nesri, M., Nounou, K., Guedida, S. E. I., Benkhoris, M. F., & Houari, A. (2024). Hybrid flatness-based control of dual star induction machine drive system for more electrical aircraft. *Power Electronics and Drives*, *9*(1), 50–62. https://doi.org/10.2478/pead-2024-0004

[22] Hussain, H. A., & Toliyat, H. A. (2017). A fault monitoring system for a reciprocating pump driven by a linear motor for oil pumping systems. In *IEEE ECCE* (pp. 4338–4344). https://doi.org/10.1109/ECCE.2017.8096747

[23] Guo, B., Liu, X., & Tan, X. (2017). Transportation systems. In *Petroleum Production Engineering* (2nd ed., pp. 275–325). Gulf Professional Publishing.

https://doi.org/10.1016/B978-0-12-809374-0.00011-8

[24] Andrada Gascón, P., & Castro, J. (2007). Solar photovoltaic water pumping system using a new linear actuator. *Renewable Energy and Power Quality*, *1*(5), 492–497. https://doi.org/10.24084/repqj05.321

[25] Pant, S., & Saini, R. P. (2020). Solar water pumping system modeling and analysis using MATLAB/Simulink. In *IEEE SCES* (pp. 1–6). https://doi.org/10.1109/SCES50439.2020.9236716

[26] Errouha, M., Motahhir, S., Combe, Q., et al. (2021). Intelligent control of induction motor for photovoltaic water pumping system. *SN Applied Sciences*, *3*, 777. https://doi.org/10.1007/s42452-021-04757-4